

# A cellular automaton technique for modelling of a binary dendritic growth with convection

Daming Li, Ruo Li, Pingwen Zhang \*

*LMAM, CCSE and School of Mathematical Science, Peking University, China*

Received 1 March 2005; accepted 12 April 2006

Available online 14 June 2006

---

## Abstract

A two-dimensional model for the simulation of a binary dendritic growth with convection has been developed in order to investigate the effects of convection on dendritic morphologies. The model is based on a cellular automaton (CA) technique for the calculation of the evolution of solid/liquid (s/l) interface. The dynamics of the interface controlled by temperature, solute diffusion and Gibbs–Thomson effects, is coupled with the continuum model for energy, solute and momentum transfer with liquid convection. The solid fraction is calculated by a governing equation, instead of some approximate methods such as lever rule method [A. Jacot, M. Rappaz, *Acta Mater.* 50 (2002) 1909–1926.] or interface velocity method [L. Nastac, *Acta Mater.* 47 (1999) 4253; L. Beltran-Sanchez, D.M. Stefanescu, *Mat. and Mat. Trans. A* 26 (2003) 367.]. For the dendritic growth without convection, mesh independency of simulation results is achieved. The simulated steady-state tip velocity are compared with the predicted values of LGK theory [Lipton, M.E. Glicksman, W. Kurz, *Metall. Trans.* 18(A) (1987) 341.] as a function of melt undercooling, which shows good agreement. The growth of dendrite arms in a forced convection has been investigated. It was found that the dendritic growth in the upstream direction was amplified, due to larger solute gradient in the liquid ahead of the s/l interface caused by melt convection. In the isothermal environment, the calculated results under very fine mesh are in good agreement with the Oseen–Ivanstov solution for the concentration-driven growth in a forced flow.

© 2006 Elsevier Inc. All rights reserved.

*Keywords:* Cellular automaton; Dendritic growth; Segregation; Continuum model; Melt convection

---

## 1. Introduction

During the last two decades, experimental techniques [1–3], analytical models [4–9] and numerical models have been developed to understand the dendritic growth and microstructure formation in alloy solidification. Deterministic and stochastic methods, which are the two main methods in numerical models, have been applied to simulate microstructure evolution. Phase field models (PFM) [10–15], where the s/l interface is described by phase-field variable, have been known as one of the most adequate deterministic models for

---

\* Corresponding author.

*E-mail addresses:* [lidaming@pku.edu.cn](mailto:lidaming@pku.edu.cn) (D. Li), [rli@math.pku.edu.cn](mailto:rli@math.pku.edu.cn) (R. Li), [pzhang@pku.edu.cn](mailto:pzhang@pku.edu.cn) (P. Zhang).

directly simulating the dendritic growth. Other notable tracking methods of s/l interface, that can be used for simulating dendritic growth, are described in details in [16,17]. The stochastic methods such as the Monte Carlo (MC) or the cellular automaton (CA) method have been developed for the prediction of macroscopic grain structure. The MC method [18] was first used to reproduce the selection of grains in the columnar zone and columnar-to-equiaxed transition (CET). However, MC method suffers from the lack of physics basis and thus cannot quantitatively analyze the effects of the various physical phenomena. In order to overcome this drawback, the CA model that accounts for the dendritic growth kinetics has been applied to simulate the solidification grain structures and CET [19–21]. Brown et al., [22] and Sasikumar et al., [23] tried to simulate thermal dendrites using the CA models. The simulation of growth for solute dendrites was also reported in Ref. [24–27]. All of these works focused on the evolution of grain structure without convection.

It has been known that forced convection in a melt has effect on dendrite growth morphologies. Beckermann et al., [28] have applied the phase field model to study the effects of melt convection on the growth of thermal dendrite in a pure melt. Recently, Lan et al., [29] have coupled Wheeler–Bottinger–McFadden (WBM) model [13] with the melt flow to study the growth of the solute dendrites, and they compared the simulation results with the classic Oseen–Ivantsov solution for the concentration-driven growth in a forced flow. Shin et al., [30] applied modified CA model to study the effects of forced convection on the morphologies of solute dendrites, but no quantitative comparison with theoretical results is given.

In the present study, a two-dimensional model of a binary dendritic growth with melt convection has been developed to investigate the effects of convection on dendritic morphologies. A continuum model for energy, solute, and momentum transfer with liquid convection, which are valid in the entire domain, was derived using the volume-averaged technique. The CA technique was used to calculate the evolution of s/l interface. Mesh independency was obtained for dendritic growth without convection and the tip velocity was compared with LGK theory. The growth of dendrite arms in a forced convection has been investigated. In the isothermal environment, the calculated results were compared with the Oseen–Ivantsov solution for the concentration-driven growth in a forced flow.

The organization of the paper is as follows. The mathematical description of the model is presented in Section 2. In Section 3, the model without melt convection is tested for mesh size independency and is compared with LGK model. The effects of melt convection on the dendritic growth is also studied, and the results is compared with Oseen–Ivantsov solution. Conclusions are given in Section 4.

## 2. Mathematical description of the model

The mathematical description of the dendritic solidification process of an alloy in two-dimensional domain ( $\Omega$ ) is depicted in Fig. 1. The s/l interface evolves in time and has to be found as part of the solution.

The alloy solidification is governed by the evolution of the temperature  $T(t, x)$ , concentration  $C(t, x)$  and melt velocity  $v_l(t, x)$ , which have to satisfy several boundary conditions at the moving s/l interface. Here we assume that the solid grain is fixed and rigid such that the velocity in solid phase  $v_s$  is zero, and that the solid and liquid density are equal.  $\psi_k$  indicates the restriction of a quantity  $\psi$  on phase  $k$  and  $\psi_{ki}$  indicates the restriction of  $\psi_k$  on s/l interface. The equations that describe the physics of the solidification process are

- Microscopic conservation equations, valid at a point within solid phase ( $k = s$ ) or liquid phase ( $k = l$ ) for any conserved quantity  $\psi$ , can be expressed as

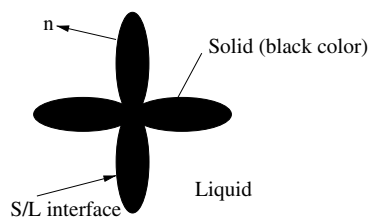


Fig. 1. Schematic representation of solidification domain  $\Omega$ .

$$\frac{\partial}{\partial t}(\rho_k \psi_k) + \nabla \cdot (\rho_k \psi_k \mathbf{v}_k) - \nabla \cdot \mathbf{J}_k = 0, \tag{1}$$

where  $\rho$  and  $\mathbf{v}$  are the density and velocity, respectively.  $\psi$  and  $J$  for the mass, momentum, energy and solute conservation are defined by

$$\begin{cases} \psi = 1, & J = 0 & \text{for mass} \\ \psi = \mathbf{v}, & J = -P & \text{for momentum} \\ \psi = h, & J = -P \cdot \mathbf{v} - \mathbf{q} & \text{for energy} \\ \psi = C, & J = -\mathbf{j} & \text{for solute} \end{cases} \tag{2}$$

where  $P$  is the total stress tensor,  $h$  the enthalpy,  $\mathbf{q}$  the heat flux and  $\mathbf{j}$  the solute flux.

- Microscopic conservation equations on s/l interface for any conserved quantity  $\psi$ , can be expressed as

$$\sum_k (\dot{m}_k \psi_k - \mathbf{n}_k \cdot \mathbf{J}_k) = 0. \tag{3}$$

Here  $\dot{m}_k = \rho_k(\mathbf{v}_k - \mathbf{w}) \cdot \mathbf{n}_k$  denotes the mass transport of convection relative to the movement of s/l interface, where  $\mathbf{w}$  is the s/l interface velocity and  $\mathbf{n}_k$  is the normal vector of s/l interface that is pointing out of phase  $k$ .

- Local equilibrium at the s/l interface

$$C_{si} = kC_{li}, \tag{4}$$

where  $k$  is the solute equilibrium partition coefficient.

- Assume that the s/l interface is in local equilibrium, the temperature  $T_i$  on s/l interface is defined by

$$T_i \stackrel{\Delta}{=} T_{li} = T_{si} = T_1^{eq} + (C_{li} - C_0)m_1 - \Gamma\kappa f(\varphi, \theta), \tag{5}$$

where  $C_0$  is the initial concentration,  $T_1^{eq}$  is the equilibrium liquidus temperature at the initial concentration,  $m_1$  is the liquidus slope,  $\Gamma$  is the Gibbs–Thomson coefficient,  $\kappa$  is the local curvature of s/l interface,  $\theta$  is the angle of the preferential growth direction with respect to a reference axis,  $\varphi$  is the angle of the normal to the s/l interface with respect to the same axis, and the anisotropy of the surface tension is described by a function  $f(\varphi, \theta)$  proposed in [27]. In Eq. (5), the s/l interface is assumed to be rough so that the kinetic time of transfer of molecules between solid and liquid is very fast compared to the characteristic diffusion time of heat or solute. Therefore, the kinetic undercooling is not accounted for in the model. Moreover, the s/l interface is assumed to be in heat equilibrium ( $T_{li} = T_{si}$ ) since the transfer time of heat is fast compared to the characteristic diffusion time of solute for the growth of solutal dendrites.

The two-domain model (1)–(5) for dendritic growth is not easy to solve, since the s/l interface should be tracked explicitly, especially for the complicated s/l interface. To overcome this shortcoming, a volume-averaged technique [31] are applied to derive the averaged conservation equations, which are valid in the entire domain. Particularly, the tracking of s/l interface is avoided since the governing equation of solid fraction is obtained by this technique.

For any space position  $x$ , an averaging volume  $V(x)$  is defined such that the shape and volume  $|V(x)|$  of  $V(x)$  is not dependent of  $x$ . For example,  $V(x)$  is the uniformly rectangular mesh and  $x$  is the center of the mesh.  $V_k(t, x)$  denotes the phase  $k$  occupied in  $V(x)$ .  $A(t, x)$  denotes the s/l interface in  $V(x)$ . The notation “ $||$ ” denotes the area in two dimensions or length in one dimension. The notation  $|V(x)|$  is replaced by  $|V|$ , since the area of  $V(x)$  is not dependent of  $x$ .

The volume average of a quantity  $\psi$  of phase  $k$  is defined by

$$\langle \psi_k \rangle(t, x) \stackrel{\Delta}{=} \frac{1}{|V|} \int_{V_k(t, x)} \psi(t, y) dy. \tag{6}$$

The volume fraction  $\epsilon_k(t, x)$  of phase  $k$  is defined by choosing  $\psi = 1$  in (6), i.e.,

$$\epsilon_k(t, x) \stackrel{\Delta}{=} \frac{|V_k(t, x)|}{|V|}. \tag{7}$$

The intrinsic volume average of  $\psi$  of phase  $k$  is defined by

$$\langle \psi_k \rangle^k(t, x) \triangleq \epsilon_k \langle \psi_k \rangle. \tag{8}$$

$\widehat{\psi}_k \triangleq \psi - \langle \psi_k \rangle^k$  denotes the fluctuation of  $\psi$ .  $\overline{\psi}_{ki}(t, x)$  indicates the average of a quantity  $\psi$  of phase  $k$  over the  $s/l$  interface:

$$\overline{\psi}_{ki}(t, x) \triangleq \frac{1}{|A_i(t, x)|} \int_{A_i(t, x)} \psi_k(t, y) dy. \tag{9}$$

Averaging (1) in  $V(x)$  yields an averaged conservation equation in phase  $k$ :

$$\begin{aligned} \frac{\partial}{\partial t} (\epsilon_k \langle \rho_k \rangle^k \langle \psi_k \rangle^k) + \nabla \cdot (\epsilon_k \langle \rho_k \rangle^k \langle \mathbf{v}_k \rangle^k \langle \psi_k \rangle^k) + \nabla \cdot \langle \rho_k \widehat{\mathbf{v}}_k \widehat{\psi}_k \rangle - \nabla \cdot (\epsilon_k \langle \mathbf{J}_k \rangle^k) + \frac{1}{|V|} \int_{A_i(t, x)} \rho_k \psi_k (\mathbf{v}_k - \mathbf{w}) \cdot \mathbf{n}_k \\ - \mathbf{J}_k \cdot \mathbf{n}_k dA = 0, \end{aligned} \tag{10}$$

for any  $(t, x)$  such that  $V(x)$  contains phase  $k$ . The physical meaning of (10) is illustrated in Appendix A. Under the assumptions in Appendix C, we get

- Mixed averaged conservation equation for energy

$$\rho C_p \frac{\partial T}{\partial t} + \rho C_p \nabla \cdot (T \epsilon_1 \langle \mathbf{v}_1 \rangle^l) = \nabla \cdot (K \nabla T) + \rho L \frac{\partial \epsilon_s}{\partial t}, \tag{11}$$

where  $C_p$  is the heat capacity,  $K$  the thermal conductivity, and  $L$  the latent heat of solidification. The following boundary condition at the walls of the domain  $\Omega$  is used:

$$-K \nabla T \cdot \mathbf{n} = h(T - T_\infty), \tag{12}$$

where  $\mathbf{n}$  is the normal to the wall,  $h$  is the coefficient of heat transfer by conduction, and  $T_\infty$  is the environment temperature.

- Mixed averaged conservation equation for solute

$$\frac{\partial C}{\partial t} + \nabla \cdot (\epsilon_1 \langle \mathbf{v}_1 \rangle^l \langle C_1 \rangle^l) = \nabla \cdot (D_1 \epsilon_1 \nabla \langle C_1 \rangle^l) + \nabla \cdot (D_s \epsilon_s \nabla \langle C_s \rangle^s), \tag{13}$$

where

$$C = \epsilon_s \langle C_s \rangle^s + \epsilon_1 \langle C_1 \rangle^l, \tag{14}$$

denotes the total solute in  $V(x)$ .  $D_1$  and  $D_s$  are the solute diffusion coefficient in liquid and solid phase, respectively. Zero flux boundary conditions are applied at the four walls of the domain  $\Omega$ . Assume that the solute is well-mixed in the liquid phase of an averaging volume (Assumption 10), i.e.,

$$\overline{C}_{li} = \langle C_1 \rangle^l, \tag{15}$$

one obtains  $\langle C_s \rangle^s$  from (14),(15) if  $\overline{C}_{li}$  is given.

- Mixed mass conservation equation

$$\nabla \cdot (\epsilon_1 \langle \mathbf{v}_1 \rangle^l) = 0. \tag{16}$$

- Averaged liquid momentum conservation equation

$$\frac{\partial (\rho_1 \epsilon_1 \langle \mathbf{v}_1 \rangle^l)}{\partial t} + \nabla \cdot (\rho_1 \epsilon_1 \langle \mathbf{v}_1 \rangle^l \langle \mathbf{v}_1 \rangle^l) + \epsilon_1 \nabla \langle p_1 \rangle^l = \nabla \cdot \{ \mu_1 \{ \nabla (\epsilon_1 \langle \mathbf{v}_1 \rangle^l) + [\nabla (\epsilon_1 \langle \mathbf{v}_1 \rangle^l)]' \} \} - M_1^d, \tag{17}$$

where  $p_1$  is the pressure in the liquid phase and the dissipative interfacial stress term is defined by [28]

$$M_1^d \triangleq h\mu_1 \frac{\epsilon_s^2}{\delta^2} \epsilon_1 \langle \mathbf{v}_1 \rangle^1. \tag{18}$$

Here  $\mu_1$  are the liquid viscosity coefficient,  $\delta$  is the thickness of s/l interface, and  $h$  is chosen to be 2.757. The drag term  $M_1^d$  vanishes in the single-phase ( $\epsilon_s = 0$  or 1).

Averaging Gibbs–Thomson Eq. (5) over  $A_i(t, x)$  yields

$$T = T_1^{\text{eq}} + (\bar{C}_{li} - C_0)m_1 - \Gamma \bar{\kappa} f(\bar{\varphi}, \theta), \tag{19}$$

by Assumption 5 and

$$\frac{1}{|A_i(t, x)|} \int_{A_i(t, x)} \kappa f(\varphi, \theta) \approx \bar{\kappa} f(\bar{\varphi}, \theta), \tag{20}$$

where  $\bar{\kappa}$  and  $\bar{\varphi}$  are the average of  $\kappa$  and  $\varphi$  over  $A_i(t, x)$ , respectively. By Assumption 16 and average Theorem (B4), we obtain

$$\hat{\mathbf{n}}_s \triangleq -\frac{\nabla \epsilon_s}{|\nabla \epsilon_s|} = (\cos \bar{\varphi}, \sin \bar{\varphi}), \quad \bar{\kappa} = \nabla \cdot \bar{\mathbf{n}}_s. \tag{21}$$

Averaging (4) over  $A_i(t, x)$  yields

$$\bar{C}_{si} = k \bar{C}_{li}. \tag{22}$$

Since the solid and liquid velocity on s/l interface vanish (Assumption 13), the solute conservation Eq. (3) ( $\psi = C, \mathbf{J} = -\mathbf{j} = \rho D \nabla C$ ) on  $A_i(t, x)$  can be written as

$$\sum_k \frac{1}{|A_i(t, x)|} \int_{A_i(t, x)} C_k \mathbf{w} \cdot \mathbf{n}_k + D_k \nabla C_k \cdot \mathbf{n}_k dA = 0. \tag{23}$$

By (22), (23), Assumption 11 and average theorem (B5) in Appendix B, we obtain

$$(\bar{C}_{li} - \bar{C}_{si}) \bar{w}_s = D_s \nabla \langle C_s \rangle^s \cdot \bar{\mathbf{n}}_s + D_1 \nabla \langle C_1 \rangle^1 \cdot \bar{\mathbf{n}}_1, \tag{24}$$

where

$$\bar{\mathbf{n}}_k \triangleq \frac{1}{|A_i(t, x)|} \int_{A_i(t, x)} \mathbf{n}_k dA = \bar{\mathbf{n}}_s, \quad k = s, 1, \tag{25}$$

by Assumption 15 and

$$\bar{w}_s = \frac{1}{|A_i(t, x)|} \int_{A_i(t, x)} \mathbf{w} \cdot \mathbf{n}_s dA. \tag{26}$$

Using the average theorem (B3), we obtain the increment of solid fraction

$$\frac{\partial \epsilon_s}{\partial t} = \frac{1}{|V|} \int_{A_i(t, x)} \mathbf{w} \cdot \mathbf{n}_s dA = \frac{|A_i(t, x)|}{|V|} \bar{w}_s. \tag{27}$$

where  $|A_i(t, x)|$  can be obtained by the assumption that the s/l interface in  $V(x)$  is straight line.

The model will be closed if five unknown variables ( $T, C, \langle \mathbf{v}_1 \rangle^1, \langle p_1 \rangle^1, \epsilon_s$ ) are solved from Eqs. (11),(13),(16),(17) and (27), respectively. The other auxiliary variables  $\bar{C}_{li}, \bar{C}_{si}, \langle C_1 \rangle^1, \langle C_s \rangle^s$  and  $\bar{w}_s$  are obtained from Eq. (19), (22), (15), (14) and (24), respectively.

### 3. Model validation

#### 3.1. Dendritic growth without convection

To show the validity of the model, the dendritic growth without melt convection for a Fe–0.6 wt% C alloy is simulated. The initial temperature and concentration are  $T_1^{\text{eq}} = 1490$  °C and  $C_0 = 0.6$  wt%, respectively.

The environment temperature  $T_\infty$  is 298 K. Other thermophysical properties used in our simulation is listed in Table 1. The square mesh  $n \times n$  is generated from the square domain  $\Omega$ .

To illustrate mesh independency, a set of numerical simulations were performed. The wall of simulated domain  $\Omega$  with the size of  $1 \times 10^{-4}$  m was cooled under a constant heat transfer coefficient  $h = 10 \text{ W/m}^{-2} \text{ K}^{-1}$ . A single grain was generated at the center of the domain, with the composition  $kC_0$ . The concentration field are shown in Fig. 2 after 0.2 s in different mesh size. It is shown that the dendritic morphology will tend to stable form with the reduction of mesh size.

The comparison with the LGK model was made for Fe-0.6% C alloy. This theory predicts a unique velocity and radius of the dendrite tip, at a given undercooling and concentration of the melt far away from the dendrite tip. To keep a constant undercooling and concentration of the melt far away the dendrite tip, the size of the simulated domain was chosen at least 3 times larger than the expected dendrite size, and the dendrite was nucleated at the center of the left wall. The initial temperature of the entire domain was that of the initial undercooling. If the left wall of the simulated domain was insulated and the latent heat of solidification was extracted from the other walls, the undercooling far away from the dendrite tip was kept almost constant. The grid size of the domain  $\Omega$  of size  $2 \times 10^{-4}$  m is  $0.5 \mu\text{m}$ . The comparison of steady-state tip velocity of our model with the LGK theory at different melt undercooling is shown in Fig. 3. It is seen that the numerical results agree well with the analytical ones.

### 3.2. Dendritic growth with convection

Fig. 4 illustrates a square physical system  $\Omega$  of size  $1 \times 10^{-4}$  m for free dendritic growth with forced convection. It is assumed that melt flows into the domain with a bulk flow velocity of  $U_{in}$  from left to right. The top and the bottom are assumed to be the symmetrical boundaries. A seed was nucleated at the center of  $\Omega$ . Thermophysical properties for Fe-0.6% C alloy listed in Table 1 is used in simulation.

In order to compare the dendritic growth without melt convection, the simulation conditions for free dendritic growth with melt convection are same as Sec.3.1. Fig. 5 shows the predicted growth morphologies and concentration field after 0.2 s, where uniform inflow velocity  $U_{in}$  is  $5 \times 10^{-4}$  m/s. Compared with the dendritic

Table 1  
Thermophysical properties for Fe-0.6 wt% C alloy used in simulation [25]

$L$ (J/kg)	$\rho$ (J/m <sup>3</sup> )	$K$ (W/m K)	$c_p$ (J/kg K)	$T_1^{eq}$ (°C)
$2.70 \times 10^5$	7300	30	800	1490
$\Gamma$ (Km)	$k$	$D_L$ (m <sup>2</sup> /s)	$D_s$ (m <sup>2</sup> /s)	$m_L$ (°C/%)
$1.9 \times 10^{-7}$	0.34	$2.0 \times 10^{-9}$	$5.0 \times 10^{-10}$	-80

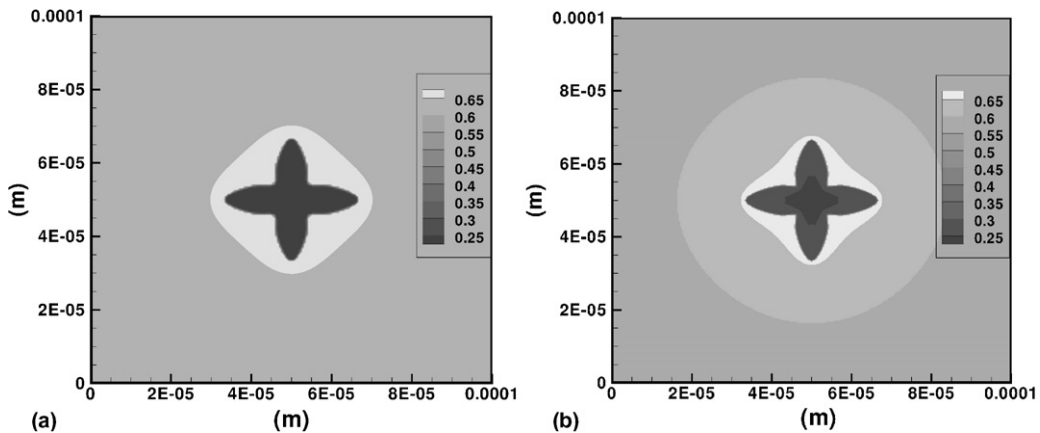


Fig. 2. Simulated concentration field C after 0.2 s, (a)  $n = 200$ , (b)  $n = 300$ .

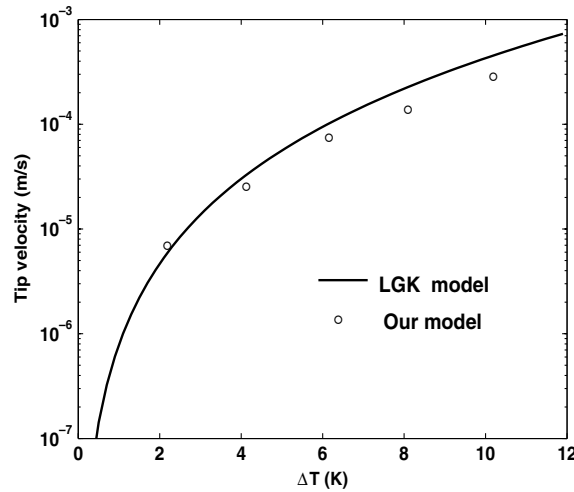


Fig. 3. Comparison of the steady-state velocity for the dendrite tip between the numerical model and the LGK theory for a Fe-0.6 wt% C alloy.

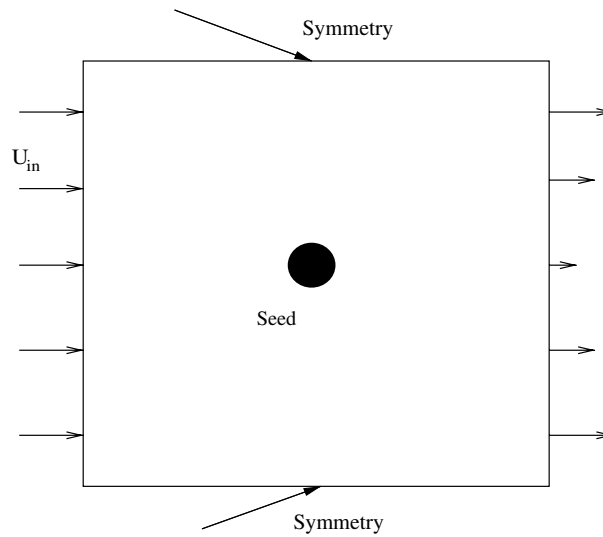


Fig. 4. Illustration of the physical system  $\Omega$  for free dendritic growth with melt convection.

morphologies without melt convection (see Fig. 2), it is found that the dendritic arm in the upstream direction grows fast, whilst the growth of the dendrite in the downstream direction is much delayed. In addition, the dendrite arms perpendicular to the bulk flow direction are slightly deflected in the upstream direction. This behavior is called “the wash away action”. The solute rejected in the liquid ahead of the s/l interface is washed away from the upstream to downstream direction, and steep concentration gradient in the upstream direction is formed, as illustrated in Fig. 6, which leads to faster growth in the upstream direction. An extension of the Ivantsov solution to the convective growth for pure alloy is derived by Bouissou and Peclec [9]. Similarly, in a isothermal environment, the Oseen–Ivantsov solution for a steady-state concentration-driven growth in a forced flow can be written as

$$\Delta = P_c \exp(P_c - P_f) \int_1^\infty \frac{\exp\{-P_c \eta + P_f [2 + \int_1^\eta g(\xi) / \sqrt{\xi} d\xi - \eta]\}}{\sqrt{\eta}} d\eta, \tag{28}$$

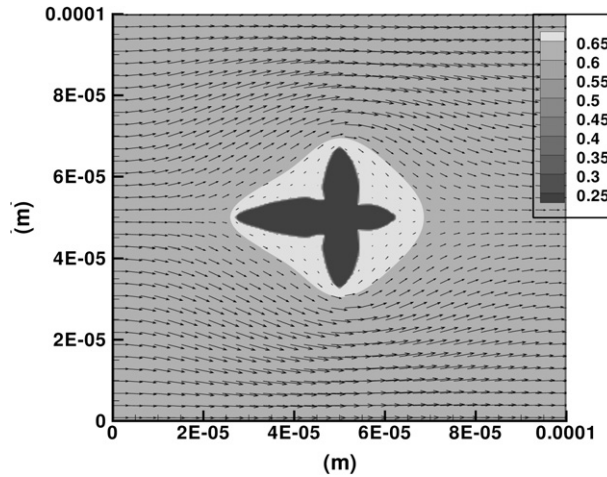


Fig. 5. The predicted growth morphologies and concentration field after 0.2 s.

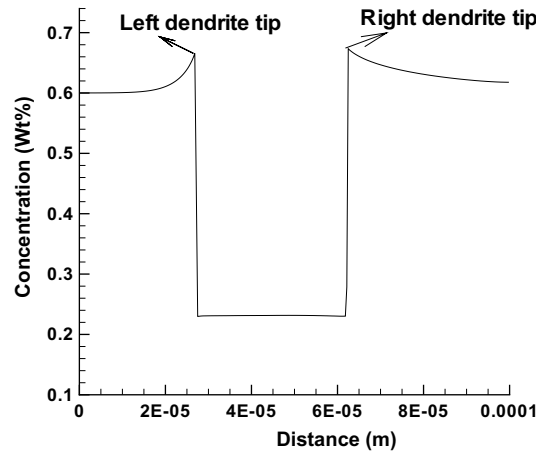


Fig. 6. Concentration profile along the primary dendrites arms.

where  $P_f$  and  $P_c$  are the flow and solute Peclet number defined by  $UR/(2D_1)$  and  $VR/(2D_1)$ , respectively. Here  $U$ ,  $R$  and  $V$  denote the bulk melt velocity  $U_{in}$ , tip radius and tip velocity in the upstream direction, respectively. The function  $g(\xi)$  is defined by

$$g(\xi) = \frac{\sqrt{\xi} \operatorname{erfc}(\sqrt{Re} \xi/2) + \sqrt{2/(\pi Re)} [\exp(-Re/2) - \exp(-Re \xi/2)]}{\operatorname{erfc}(\sqrt{Re}/2)}, \tag{29}$$

where Reynold number  $Re$  is defined by  $UR\rho/\mu_l$ . The driving force for solute dendritic growth is defined by

$$\Delta = \frac{C_{li} - C_l^\infty}{C_{li} - C_{si}}, \tag{30}$$

where  $C_l^\infty$  is the liquid concentration far away from the tip. In a constant undercooling environment  $\Delta T = 3$  K, a seed is nucleated in the center of  $\Omega$  of size  $1 \times 10^{-4}$  m. The comparison between simulation values and Oseen–Ivantsov solution is illustrated in Table 2, where  $\Delta_{P_c}$  and  $\Delta_{SI}$  are obtained by Oseen–Ivantsov solution (28) and the definition of driving force (30), respectively. In order to estimate the local tip radius, a fourth-order polynomial was used to fit the dendrite tip in the upstream direction within a half of primary arm distance. For the coarse mesh ( $n = 200$ ), the relative error of the simulated driving force  $\Delta_{SI}$  is about 26%.

Table 2

Comparison between simulation values and Oseen–Ivantsov solution, Error =  $|\Delta_{Pc} - \Delta_{SI}|/\Delta_{Pc}$

$n$	$U$ (m/s)	$V$ (m/s)	$R$ (m)	$P_c$ (-)	$P_f$ (-)	$Re$	$C_i$ (wt%)	$\Delta_{SI}$ (-)	$\Delta_{Pc}$ (-)	Error (-)
200	$5 \times 10^{-4}$	$4.87 \times 10^{-5}$	$9.841 \times 10^{-7}$	0.012	0.123	0.006	0.633	0.079	0.058	26%
300	$5 \times 10^{-4}$	$5.47 \times 10^{-5}$	$8.331 \times 10^{-7}$	0.0114	0.104	0.005	0.629	0.072	0.061	16%

The relative error was decreased to be 16% for the fine mesh ( $n = 300$ ), which shows that the agreement between the model and Oseen–Ivantsov solution will be achieved with the reduction of mesh size.

#### 4. Conclusions

A quantitative CA model for simulating a binary dendritic growth with convection is presented. Heat conduction, solute diffusion and melt flow, which are valid in the entire simulation domain, are coupled with the evolution of s/l interface in the model. Mesh independency of simulation results is achieved for the dendritic growth without melt convection. Moreover, the simulated tip velocity agrees well with the predicted values of the LGK theory for free dendritic growth in large range of undercooling melt. Compared with the dendritic growth without convection, the phenomena of “the wash away action” is rather obvious in the free dendritic growth in the forced convection, which leads to faster growth in the upstream direction. Although it is difficult to obtain mesh independency for simulating the convective growth in an non-isothermal environment due to the restriction of computational time, the simulated steady-state driving force of convective growth in an isothermal environment agrees well with Oseen–Ivantsov solution with the reduction of mesh size. To obtain more precise comparison with the theoretical results, it is necessary to use adaptive technique to reduce the computational time.

#### Acknowledgement

This work was supported by the Integrated Simulation of Material Production Processing and Technological Organization Properties for New-aged Iron and Steel (No. 2001AA339030), the National Science Foundation of China (No. 10271112), the Special Funds for Major State Basic Research (No. G1999032804), the Joint Applied Mathematics Research Institute between Peking University and Hong Kong Baptist University, and Shanghai Jiaotong University youth funds.

#### Appendix A. Physical meaning of (10)

From Assumption 1, we have

$$\langle \hat{\rho}_k \hat{\psi}_k \rangle^k = 0, \quad \langle \rho_k \hat{v}_k \hat{\psi}_k \rangle^k = \langle \rho_k \rangle^k \langle \hat{v}_k \hat{\psi}_k \rangle^k. \tag{A1}$$

Under the assumption of (A1), the physical meaning of every term in (10) is illustrated as follows:

- The increment of  $\psi$  in  $V_k(t, x)$

$$\frac{\partial}{\partial t} (\epsilon_k \langle \rho_k \rangle^k \langle \psi_k \rangle^k) = \frac{\partial}{\partial t} \left( \frac{1}{|V|} \int_{V_k} \rho_k \psi_k dV \right). \tag{A2}$$

- The amount of flux from  $V_k(t, x)$  through  $\partial V_k(t, x) \setminus A_i(t, x)$ , where  $\partial V_k(t, x)$  denotes the boundary of  $V_k(t, x)$ ,

$$\nabla \cdot (\epsilon_k \langle \rho_k \rangle^k \langle \mathbf{v}_k \rangle^k \langle \psi_k \rangle^k) + \nabla \cdot (\langle \rho_k \hat{\mathbf{v}}_k \hat{\psi}_k \rangle) = \frac{1}{|V|} \int_{\partial V_k(t, x) \setminus A_i(t, x)} \rho_k \psi_k \mathbf{v}_k \cdot \mathbf{n}_k dA. \tag{A3}$$

- The action of  $J$  on  $\partial V_k(t, x) \setminus A_i(t, x)$

$$\nabla \cdot (\epsilon_k \langle J_k \rangle^k) = \frac{1}{|V|} \int_{\partial V_k(t, x) \setminus A_i(t, x)} J_k \cdot \mathbf{n}_k dA. \tag{A4}$$

- The action of  $J$  of phase  $k$  on  $A_i(t, x)$

$$\frac{1}{|V|} \int_{A_i(t, x)} J_k \cdot \mathbf{n}_k dA. \tag{A5}$$

- The increment of  $\psi$  in  $V_k(t, x)$  due to the fluid velocity relative to the s/l interface velocity  $\mathbf{w}$  in  $V(x)$

$$\frac{1}{|V|} \int_{A_i(t, x)} \rho_k \psi_k (\mathbf{v}_k - \mathbf{w}) \cdot \mathbf{n}_k dA. \tag{A6}$$

**Appendix B. Averaging theorem**

For any  $(t, x)$ , such that  $A_i(t, x)$  is contained in  $V(x)$ , we have

$$\left\langle \frac{\partial \psi_k}{\partial t} \right\rangle = \frac{\partial \langle \psi_k \rangle}{\partial t} - \frac{1}{|V|} \int_{A_i(t, x)} \psi_k \mathbf{w} \cdot \mathbf{n}_k dA, \tag{B1}$$

$$\langle \nabla \psi_k \rangle = \nabla \langle \psi_k \rangle + \frac{1}{|V|} \int_{A_i(t, x)} \psi_k \mathbf{n}_k dA. \tag{B2}$$

Especially,

$$\frac{\partial \epsilon_k}{\partial t} = \frac{1}{|V|} \int_{A_i(t, x)} \mathbf{w} \cdot \mathbf{n}_k dA, \tag{B3}$$

$$\nabla \epsilon_k = -\frac{1}{|V|} \int_{A_i(t, x)} \mathbf{n}_k dA, \tag{B4}$$

$$\langle \nabla \psi_k \rangle = \epsilon_k \nabla \langle \psi_k \rangle^k + \frac{1}{|V|} \int_{A_i(t, x)} \widehat{\psi}_k \mathbf{n}_k dA, \tag{B5}$$

$$\frac{1}{|V|} \int_{A_i(t, x)} \langle \psi_k \rangle^k \mathbf{n}_k dA = -\langle \psi_k \rangle^k \nabla \epsilon_k. \tag{B6}$$

**Appendix C. Assumptions of the model**

**Assumption 1.** Density in solid and liquid phase ( $\rho_s, \rho_l$ ) are constant, respectively, i.e.,  $\rho_s = \rho_l \stackrel{\Delta}{=} \rho$ .

**Assumption 2.** Thermal conductivity coefficients in solid and liquid phase ( $K_s, K_l$ ) are constant, respectively, i.e.,  $K_s = K_l \stackrel{\Delta}{=} K$ . Moreover, the liquid thermal capacity  $C_p$  is constant.

**Assumption 3.** The effect of stress work on the transport of energy is omitted, i.e.,

$$\nabla \cdot (P_k \cdot \mathbf{v}_k) = 0. \tag{C1}$$

**Assumption 4.** Fourier thermal conductivity law holds, i.e.,

$$\mathbf{q}_k = -K_k \nabla T_k, \quad k = 1, s. \tag{C2}$$

**Assumption 5.** The solid and liquid phases within an averaging volume are in thermal equilibrium, i.e.,

$$T \stackrel{\Delta}{=} \overline{T}_{ki} = \langle T_k \rangle^k, \quad k = s, l. \tag{C3}$$

**Assumption 6.** The enthalpy in liquid phase are assumed to vary with temperature, and the difference of averaged liquid and solid enthalpy is given, i.e.,

$$\begin{cases} h_l = C_p T_1 \\ L \triangleq \langle h_l \rangle^l - \langle h_s \rangle^s \end{cases} \quad (C4)$$

**Assumption 7.** The thermal fluctuation can be omitted, i.e.,

$$\int_{A_i(t,x)} \widehat{T}_k \mathbf{n}_k dA = 0, \quad k = 1, s. \quad (C5)$$

**Assumption 8.** Ficker diffusion law holds, i.e.,

$$\mathbf{j}_k = -\rho_k D_k \nabla C_k, \quad k = 1, s. \quad (C6)$$

**Assumption 9.** Solute diffusion coefficients in solid and liquid phase are constants, respectively.

**Assumption 10.** The solute is well-mixed in the liquid phase of an averaging volume, i.e.,

$$\bar{C}_{li} = \langle C_l \rangle^l. \quad (C7)$$

**Assumption 11.** The solute fluctuation can be omitted, i.e.,

$$\begin{cases} \int_{A_i(t,x)} \widehat{C}_k \mathbf{n}_k dA = 0 \\ \int_{A_i(t,x)} (C_k - \bar{C}_{ki})(\mathbf{w} \cdot \mathbf{n}_k) dA = 0 \\ \int_{A_i(t,x)} (\nabla C_k - \langle \nabla C_k \rangle^k) \cdot \mathbf{n}_k dA = 0 \end{cases} \quad (C8)$$

**Assumption 12.** The pressure equilibrium holds in the liquid phase of an averaging volume, i.e.,

$$\bar{p}_{li} = \langle p_l \rangle^l. \quad (C9)$$

**Assumption 13.** The velocity in the solid phase and liquid velocity on the s/l interface are zero, i.e.,

$$\mathbf{v}_s = 0, \quad \mathbf{v}_{li} = 0. \quad (C10)$$

**Assumption 14.** Dispersive flux is omitted, i.e.,

$$\langle \rho_k \widehat{\mathbf{v}}_k \widehat{\psi}_k \rangle = 0, \quad \psi = C, h, \mathbf{v}. \quad (C11)$$

**Assumption 15.** Liquid phase can be seen as Newtonian fluid, the fluctuation of shear stress at the s/l interface is omitted, and average liquid friction at the s/l interface is proportional to the liquid viscosity  $\mu_l$  and velocity gradient, i.e.,

$$\tau_l = \mu_l (\nabla \mathbf{v}_l + (\nabla \mathbf{v}_l)^t), \quad (C12)$$

$$\int_{A_i(t,x)} (\tau_l - \bar{\tau}_{li}) \cdot \mathbf{n}_k dA = 0, \quad (C13)$$

$$\bar{\tau}_{li} \cdot \left( \frac{-\nabla \epsilon_s}{|\nabla \epsilon_s|} \right) = h \mu_l \epsilon_s \frac{\langle \mathbf{v}_l \rangle^l}{\delta}. \quad (C14)$$

The analytical solution of one-dimensional phase field model

$$\epsilon_s = \frac{1}{2} \left( 1 - \tanh \frac{n}{2\delta} \right) \quad (\text{C15})$$

is used to approximate  $\nabla \epsilon_s$  in the dissipative interfacial stress term  $M_1^d = \frac{1}{|V|} \int_{A_i(t,x)} \tau_1 \cdot \mathbf{n}_1 dA \approx \bar{\tau}_{li} \cdot \nabla \epsilon_s$ . In Eq. (C15),  $n$  is the distance to the s/l interface and  $\delta$  is the thickness of s/l interface.

**Assumption 16.** The s/l interface in an averaging volume  $V(x)$  is approximated by a straight line.

## References

- [1] M.E. Glicksman, E. Winsa, R.C. Hahn, T.A. Lograsso, S.H. Tirmizi, M.E. Selleck, *Metall. Trans.* 19(A) (1987) 1945.
- [2] M.A. Chopra, M.E. Glicksman, M.B. Singh, *Metall. Trans.* 19(A) (1988) 3087.
- [3] D.G. McCartney, J.D. Hunt, *Acta Metall.* 29 (1981) 1851.
- [4] W. Kurz, D.J. Fisher, *Fundamentals of Solidification*, third ed., Trans Tech Publications., Aedermannsdorf, Switzerland, 1989.
- [5] W. Kurz, B. Giovanola, R. Trivedi, *Metall. Trans. A* 18(A) (1987) 823.
- [6] J. Lipton, M.E. Glicksman, W. Kurz, *Metall. Trans.* 18(A) (1987) 341.
- [7] J. Lipton, W. Kurz, R. Trivedi, *Acta Metall.* 35 (1987) 957.
- [8] R. Trivedi, W. Kurz, *Acta Metall. Mater.* 42A (1994) 15.
- [9] Ph. Bouissou, P. Pelce, *Phys. Rev. A* 40 (1989) 6673.
- [10] A.A. Wheeler, W.J. Boettinger, G.B. McFadden, *Phys. Rev. A* 45 (1992) 7424.
- [11] A.A. Wheeler, B.T. Murray, R.J. Schaefer, *Physics D* 66 (1993) 243.
- [12] S.L. Wang, R.F. Sekerka, A.A. Wheeler, B.T. Murray, S.R. Coriell, R.J. Braun, G.B. McFadden, *Physics D* 69 (1993) 189.
- [13] J.A. Warren, W.J. Boettinger, *Acta Metall.* 43 (1995) 689.
- [14] S.G. Kim, W.T. Kim, T. Suzuki, *Phys. Rev. E* 58 (1998) 3316.
- [15] S.G. Kim, W.T. Kim, T. Suzuki, *Phys. Rev. E* 60 (1999) 7186.
- [16] W. Shyy, H.S. Udaykumar, M.M. Rao, R.W. Smith, *Computational Fluid Dynamics with Moving Boundaries*, Taylor and Francis, London, 1996.
- [17] H.S. Udaykumar, W. Shyy, *Int. J. Heat Mass Transfer* 38 (11) (1995) 2057.
- [18] S.G.R. Brown, J.A. Spittle, *Mater. Sci. Technol.* 5 (1989) 362.
- [19] M. Rappaz, Ch.-A. Gandin, *Acta Metall.* 41 (1993) 345.
- [20] Ch.-A. Gandin, M. Rappaz, *Acta Metall. Mater.* 42 (1994) 2233.
- [21] Ch.-A. Gandin, J.L. Desbiolles, M. Rappaz, Ph. Thevoz, *Metall. Mater. Trans. A* 30A (1999) 3153.
- [22] S.G.R. Brown, T. Williams, J.A. Spittle, *Acta Metall.* 42 (1994) 2893.
- [23] R. Sasikumar, R. Sreenivasan, *Acta Metall.* 42 (1994) 2381.
- [24] U. Dilthey, V. Pavlik, T. Reichel, in: H. Cerjak, H.K.D.H. Bhadeshia (Eds.), *Mathematical Modeling of Weld Phenomena 3*, The Institute of Materials, London, 1997, pp. 85–105.
- [25] L. Nastac, *Acta Mater.* 47 (1999) 4253.
- [26] A. Jacot, M. Rappaz, *Acta Mater.* 50 (2002) 1909–1926.
- [27] L. Beltran-Sanchez, D.M. Stefanescu, *Mat. and Mat. Trans. A* 26 (2003) 367.
- [28] C. Beckermann, H.J. Diepers, I. Steibach, A. Kamma, X. Tong, *J. Comp. Phys.* 154 (1999) 468.
- [29] C.W. Lan, C.J. Shih, *Phys. Rev. E* 69 (2004) 031601-1.
- [30] Y.H. Shin, C.P. Hong, *ISIJ Int.* 42 (2002) 359–367.
- [31] M. Schneider, C. Beckermann, *Metall. Trans. A* 26 (1995) 2373.